ANTICANCER RESEARCH *41*: 583-599 (2021)
doi:10.21873/anticanres.14810

Acquisition of Letrozole Resistance Through Activation of the p38/MAPK Signaling Cascade

RASHIDRA R. WALKER[1], KAREN M. GALLEGOS[1], MELYSSA R. BRATTON[2], KITANI P. LEMIEUX[3], KUN ZHANG[4], GUANGDI WANG[5], A. MICHAEL DAVIDSON[1] and SYREETA L. TILGHMAN[1]

[1]*Division of Pharmaceutical Sciences, College of Pharmacy and Pharmaceutical Sciences, Florida A&M University, Tallahassee, FL, U.S.A.;*
[2]*Biospecimens Core Laboratory, Louisiana Cancer Research Center, New Orleans, LA, U.S.A.;*
[3]*Division of Basic Pharmaceutical Sciences, College of Pharmacy, Xavier University of Louisiana, New Orleans, LA, U.S.A.;*
[4]*Division of Mathematical and Physical Sciences, Department of Computer Science, College of Arts and Sciences, Xavier University of Louisiana, New Orleans, LA, U.S.A.;*
[5]*Division of Mathematical and Physical Sciences, Department of Chemistry, College of Arts and Sciences, Xavier University of Louisiana, New Orleans, LA, U.S.A.*

Abstract. *Background/Aim: Previous reports identified a global proteomic signature of estrogen-independent letrozole resistant breast cancer cells, however, it remains unclear how letrozole-resistance is impacted when cells remain estrogen receptor positive (ER+). Materials and Methods: To capture the protein expression profile associated with ER+ Aromatase inhibitor (AI) resistance, a global proteomic analysis was conducted using the letrozole-sensitive (T47Darom cells) and letrozole-resistant cells (T47DaromLR cells). To examine the molecular features associated with this phenotype Kaplan–Meier analysis, phospho-antibody arrays, proliferation and apoptosis assays were conducted. Results: MAP3K6 was up-regulated in the T47DaromLR cells by 3.2-fold ($p<0.01$) which was associated with a decrease in relapse-free survival among breast cancer patients ($p=0.0019$). Members of the MAPK/p38 pathway (i.e., phospho-MKK6, phospho-p38, phospho-RSK1, phospho-RSK2, and p70S6K MAPK) were also increased in the T47DaromLR cells, while inhibiting p38 led to decreased proliferation and induction of apoptosis. Conclusion: Activation of the p38/MAPK pathway leads to ER+ AI-resistance.*

Correspondence to: Syreeta L. Tilghman, Ph.D., Division of Pharmaceutical Sciences, College of Pharmacy and Pharmaceutical Sciences, Florida A&M University, 1415 Martin Luther King Jr. Blvd Tallahassee, FL, 32307, U.S.A. Tel: +1 8505993933, e-mail: syreeta.tilghman@famu.edu

Key Words: Breast cancer, letrozole, aromatase inhibitor, resistance, p38, and MAPK.

Aromatase inhibitors, like letrozole, are the first-line therapy for postmenopausal women with estrogen-dependent breast cancer. These agents block the biosynthesis of estrogen through aromatase inhibition and inhibit the proliferation of estrogen-dependent breast tumors. Unfortunately, after several years some patients develop therapeutic resistance, and the tumors continue to proliferate. To study aromatase inhibitor resistance in the laboratory setting, a letrozole resistant cell line was developed by inoculating the MCF-7Ca cells (MCF-7 cells stably transfected into the human aromatase gene) into immunocompromised mice and treating the mice with letrozole for 56 weeks (1). After long-term treatment, the tumors acquired resistance to letrozole, were cultured *in vitro* and termed long term letrozole treated (LTLT)-Ca cells. Previous studies in our lab have demonstrated that as the letrozole-sensitive cells (AC-1) transition to the letrozole-resistant phenotype (LTLT-Ca) they are associated with estrogen independence, up-regulation of growth factor signaling cascades, and increased motility (2). However, the changes that occur as cells acquire resistance to letrozole while maintaining estrogen dependence remains unclear.

To this end, an *in vitro* model of letrozole resistance was developed whereby the T47D parental cell line was stably transfected with the human aromatase gene and termed the T47Darom cells. The T47Darom cells were treated with letrozole for 75 weeks until they became resistant to letrozole and were called T47DaromLR cells. When the T47DaromLR cells were characterized, they retained both aromatase activity and ER expression (3). As such, this was an ideal model to test the hypothesis that there are distinct proteomic profiles between estrogen-dependent and estrogen-independent letrozole resistant breast cancer cells,

which may be useful for therapeutic decision making. Here, we examined the proteomic signature associated with T47D cells as they acquire resistance to an aromatase inhibitor.

Materials and Methods

Cell culture. In this study, we utilized two cell lines previously developed and derived from the T47D parental breast cancer cell line (3). The T47Darom cells (the T47D cells stably transfected with the human aromatase gene) were cultured and maintained in phenol red DMEM media (Invitrogen, Waltham, MA, USA) supplemented with 5% fetal bovine serum (FBS), penicillin-streptomycin, antimycotic-antibiotic (10,000 U/ml penicillin G sodium; 10,000 mg/ml streptomycin sulfate), and 0.75 mg/ml geneticin (Invitrogen). The T47DaromLR cells were generated by treating the T47Darom for 75 weeks in the presence of 10 μM letrozole and were maintained in phenol red-free DMEM media (Invitrogen) supplemented with 10% charcoal-stripped fetal bovine serum (FBS), penicillin-streptomycin, antimycotic-antibiotic (10,000 U/ml penicillin G sodium; 10,000 mg/ml streptomycin sulfate), 7.5 mg/ml geneticin (Invitrogen), and 1 mM letrozole (Sigma-Aldrich, St. Louis, MO, USA). The cells were maintained in a tissue culture incubator in a humidified atmosphere of 5% CO_2 and 95% air at 37˚C. Both cell lines were a generous gift from ITT Research Institute.

MAPK and RTK phosphorylation antibody arrays. To compare the changes in activation/phosphorylation of MAPK and Receptor Tyrosine Kinases (RTK) between the T47Darom and T47DaromLR cells, the Human MAPK Phosphorylation Antibody Array (ab211061, Abcam, Cambridge, MA, USA) and the Human RTK Phosphorylation Antibody Array Membrane (ab193662, Abcam), were evaluated respectively. The antibody arrays consisted of nitrocellulose membranes containing anti-MAPK or anti-RTK antibodies spotted duplicate and include positive and negative controls and a blank. Cell lysates were prepared from T47Darom and T47DaromLR cells using Cell Lysis Buffer supplemented with Phosphatase Inhibitor and Protease Inhibitor Cocktail and stored at −80˚C until use. For each cell lysate, 900 μg of total protein were determined by the Bradford Assay (BioRad, Hercules, CA, USA) and incubated in 2 ml of 1X Blocking Buffer at room temperature for 30 min. The antibody array membranes were washed and subsequently incubated with Detection Antibody Cocktail (for MAPK assays) or with biotinylated anti-phosphotyrosine antibody (for RTK assays) overnight at ˚C to detect phosphorylated cytokines or tyrosine on activated receptors. After washing and incubation with HRP-streptavidin, the membranes were subjected to visualization with chemiluminescence-based detection method.

Cell lysis. T47Darom and T47DaromLR control cells were cultured to 80% confluence in standard growth medium as described above and washed three times with cold Hank's Buffered Salt Solution (HBSS), then collected with a cell scraper. Nonidet P-40 cell lysis buffer (Invitrogen) containing an additional 1 mM of phenylmethyl sulfonyl fluoride (PMSF) and protease inhibitor mixture (Sigma-Aldrich) was used to extract total cellular proteins. The concentration of proteins was measured with BCA assay (Pierce Biotechnology, Rockford, IL, USA). The cell lysates were stored at –80˚C before further processing.

Trypsin digestion. Protein samples were digested with sequencing grade modified trypsin (Promega Corp, Madison, WI, USA) according to the manufacturer's instructions. Briefly, to aliquots of 100 μg of protein sample were added 45 μl of 200 mM triethylammonium bicarbonate (TEAB) and the final volume was adjusted to 100 μl with ultrapure water. Five microliters of 200 mM Tris (2-carboxyethyl) phosphine (TCEP) were added and the resulting mixture was incubated for 1 h, then 5 μl of 375 mM iodoacetamide were added and the mixture was incubated for 30 min in the dark. After incubation, 1 ml of prechilled acetone was added and the precipitation was allowed to proceed overnight. The acetone-precipitated protein pellets were suspended with 100 μl of 200 mM TEAB and 2.5 μg of trypsin were added to digest the sample overnight at 37˚C.

Tandem mass tags (TMT) labeling. Tandem mass tags TMT6 (Thermo Scientific, Waltham, MA, USA) with different molecular weights (126~131 Da) were applied as isobaric tags for relative and absolute quantification. According to the manufacturer's protocols, the digested samples were individually labeled with TMT6 reagents for 1 h as follows: three 100-μg aliquots of digested peptides from the T47Darom cells were each labeled with a different isobaric tag (TMT126, 127, and 128, respectively). Likewise, 100 μg aliquots of peptides from the T47DaromLR cells were labeled with TMT129, 130, and 131 mass tags, respectively. The labeling reaction was quenched with 5% hydroxylamine. Finally, the six labeled peptide aliquots were combined for subsequent fractionation.

Fractionation of labeled peptide mixture using a strong cation exchange column. The combined TMT labeled peptide mixture was fractionated with a strong cation exchange column (SCX) (Thermo Scientific) on a Shimadzu 2010 HPLC equipped with a UV detector (Shimadzu, Columbus, MD, USA). The mobile phase consisted of buffer A (5 mM KH_2PO_4, 25% acetonitrile, pH 2.8) and buffer B (buffer A plus 350 mM KCl). The column was equilibrated with buffer A for 30 min before sample injection. The mobile phase gradient was set as follows at a flow rate of 1.0 ml/min: (a) 0 to 10 min: 0% buffer B; (b) 10 to 40 min: 0% to 25% buffer B, (c) 40 to 45 min: 25% to 100% buffer B; (d) 45 to 50 min: 100% buffer B; (e) 50 to 60 min: 100% to 0% buffer B; (f) 60 min to 90 min: 0% buffer B. A total of 60 fractions were initially collected, lyophilized, and combined into 15 final fractions based on SCX chromatographic peaks.

Desalination of fractionated samples. A C18 solid-phase extraction (SPE) column (Hyper-Sep SPE Columns, Thermo-Fisher Scientific) was used to desalt all collected fractions. The combined 15 fractions were each adjusted to 1 ml final volume containing 0.25% (v/v in water) trifluoroacetic acid (TFA, Sigma-Aldrich). The C18 SPE columns were conditioned before use by filling them with 1 ml acetonitrile and allowing the solvent to pass through the column slowly (~3 min). The columns were then rinsed three times with 1 ml 0.25% (v/v in water) TFA solution. The fractions were loaded on to the top of the SPE cartridge and allowed to elute slowly. Columns were washed four times with 1-ml 0.25% TFA aliquots before the peptides were eluted with 3×400 μl of 80% acetonitrile/0.1% formic acid (aqueous).

LC-MS/MS analysis on LTQ-Orbitrap. Peptides were analyzed on an LTQ-Orbitrap XL instrument (Thermo-Fisher Scientific) coupled to an Ultimate 3000 Dionex nanoflow LC system (Dionex,

Sunnyvale, CA, USA). High mass resolution was used for peptide identification and high energy collision dissociation (HCD) was employed for reporter ion quantification. The RP-LC system consisted of a peptide Cap- rap cartridge (0.5×2 mm) (Michrom BioResources, Auburn, CA, USA) and a prepacked BioBasic C18 PicoFrit analytical column (75 μM i.d. ×15 cm length, New Objective, Woburn, MA, USA) fitted with a For-tisTip emitter tip. Samples were loaded onto the trap cartridge and washed with mobile phase A (98% H_2O, 2% acetonitrile, and 0.1% formic acid) for concentration and desalting. Subsequently, peptides were eluted over 180 min from the analytical column *via* the trap cartridge using a linear gradient of 6-100% mobile phase B (20% H_2O, 80% acetonitrile, and 0.1% formic acid) at a flow-rate of 0.3 μl per min using the following gradient: 6% B for 5 min; 6-60% B for 125 min; 60-100% B for 5 min; hold at 100% B for 5 min; 100-6% B in 2 min; hold at 6% B for 38 min.

The LTQ-Orbitrap tandem mass spectrometer was operated in a data-dependent mode. Briefly, each full MS scan (60,000 resolving power) was followed by six MS/MS scans where the three most abundant molecular ions were dynamically selected and fragmented by collision-induced dissociation (CID) using a normalized collision energy of 35%, and the same three molecular ions were also scanned three times by HCD-MS2 with collision energy of 45%. MS scans were acquired in profile mode and MS/MS scans in centroid mode. LTQ-Orbitrap settings were as follows: spray voltage 2.0 kV, 1 microscan for MS1 scans at 60,000 resolutions (fwhm at *m/z* 400), microscans for MS2 at 7500 resolutions (fwhm at *m/z* 400); full MS mass range, *m/z* 400-1400; MS/MS mass range, *m/z* 100-2000. The "FT master scan preview mode," "Charge state screening", "Monoisotopic precursor selection" and "Charge state rejection" were enabled so that only the 2+, 3+, and 4+ ions were selected and fragmented by CID and HCD.

Database search and TMT quantification. The protein search algorithm used was Mascot v2.3.01 (Matrix Science, Boston, MA, USA). Mascot format files were generated by the Proteome Discoverer 1.2 software (Thermo-Fisher Scientific) using the following criteria: database, *IPI_Human.fasta. v3.77* (containing 89,422 entries and concatenated with the reversed versions of all sequences.); enzyme, trypsin; maximum missed cleavages, 2; Static modifications, carbamido- methylation (+57 Da), N-terminal TMT6plex (+229 Da), lysyl TMT6plex (+229 Da). Dynamic modifications, N-terminal Clnpyro- Glu (+17 Da); methionine oxidation (+16 Da); STY phosphorylation (+80 Da); Precursor mass tolerance was set at 20 ppm; fragment match tolerance was set at 0.8 Da. Peptides reported by the search engine were accepted only if they met the false discovery rate of $p<0.05$ (target decoy database), a Mascot ion score ≥30 for peptide identifications was required. For TMT quantification, the ratios of TMT reporter ion abundances in MS/MS spectra generated by HCD (up to six reporter ions ranging from *m/z* 126.12 to *m/z* 131.14) from raw data sets were used to calculate fold changes in proteins between control and treatment.

Kaplan–Meier (KM) survival analysis. The application of KM plot has been described in detail previously (4). Briefly, KM plots were obtained using the KM Plotter web-based (kmplot.com/analysis) curator, which surveys public microarray repositories for relapse-free and overall survival among patients with breast, lung, ovarian or gastric cancers. The KM Plotter recognizes 54,675 individual Affymetrix probe sets, and surveys expression data from 4,142 breast cancer patients (as of 2014). Survival and gene expression data were derived from the GEO (Gene Expression Omnibus), TCGA (The Cancer Genome Atlas), and EGA (European Genome-phenome Atlas) databases. In order to ascertain P4HB expression, Affymetrix probe 200654 was selected. Overall Survival in the total population (1402 patients) was determined.

Viability assay. Proliferation assays were performed as previously described (5). Specifically, the T47Darom cells (aromatase inhibitor sensitive) were plated in 96-well plates at a density of 2×10^3 cells per well for each cell line and allowed to recover for 24 h. The T47DaromLR cells (AI-resistant) were cultured in the presence of letrozole. For proliferation assays, the cells were treated with DMSO (control) or 30 μM SB205380 in 96-well plates to determine the effects of the various treatments in the absence of letrozole. The resazurin dye (Sigma-Aldrich) was added to each well at 10% of the total volume and measured at 24 h. The SpectraMax® MiniMax® 300 Imaging Cytometer (Molecular Devices, San Jose, CA, USA) was used to measure fluorescence and background wavelengths at 530 nm and 590 nm to determine proliferation. All experiments were performed with n ≥3 and a total of 3 biological replicates were performed. The proliferative activity was calculated as a percent of the vehicle controls as follows:

Antiproliferative activity=[Fluorescence of viable cells (control) − Fluorescence of viable cells (treated)]/Fluorescence of viable cells (control).

Caspase 3/7 apoptosis assay. The T47Darom and T47DaromLR cells were seeded at a density of 1.5×10^3 cells in a 96-well plate with appropriate media overnight. Cells were treated the following day with DMSO (control) or 10 μM SB205380. Cells were incubated for 24 h at 37˚C with 5% CO_2. On the following day, the cells treated with 4 μM CellEvent™ Caspase-3/7 Green Detection Reagent (Invitrogen) and incubated for 30 min at 37˚C with 5% CO_2. The cells were then fixed with 4% formaldehyde and allowed to incubate for 15 min at room temperature. The SpectraMax®MiniMax® 300 Imaging Cytometer (Molecular Devices) was used to measure fluorescence and background wavelengths at 530 nm and 502 nm, respectively. Cells were imaged on Nikon Ti Eclipse microscope (Minato, Tokyo, Japan) using a FITC filter.

Results

Proteomic profile of estrogen-dependent letrozole resistant breast cancer cells is associated with a unique signature. To examine the global changes in protein expression as cells transition from AI-sensitive to AI-resistant while maintaining ER expression, a gel-free proteomic approach combining tandem mass tag (TMT) labeling, two-dimensional HPLC, and high-resolution mass spectrometry was utilized. The identities of over 1900 proteins with quantitative abundance ratios were present in both the letrozole sensitive (T47Darom) and the letrozole resistant (T47DaromLR) breast cancer cells. Abundance ratios ≥1.25 were defined as high while those ≤0.8 were defined as low. Of the quantified proteins, a total of 127 were significantly high ($p<0.05$) as

indicated by Table I, while 111 were significantly low ($p<0.05$) as shown by Table II. The top three up-regulated proteins were mitogen-activated kinase kinase kinase 6 (M3K6), protein disulfide isomerase (P4HB), and midasin (MDN1), and they were increased by 3.204-fold ($p<0.01$), 3.195-fold ($p<0.01$), and 2.759-fold ($p<0.001$), respectively. These proteins are indicated in bold. Among the down-regulated proteins, Peptidyl-prolyl cis-trans isomerase (FKBP4) was decreased by 0.484-fold ($p<0.001$) which is also indicated in bold.

High MAP3K6 expression is associated with decreased relapse-free survival. Since MAP3K6 was significantly increased, we sought to examine the clinical relevance on patient survival. To predict whether increased MAP3K6 expression levels were associated with differences in survival, KM Plotter was used to interrogate publicly available microarray repositories of breast cancer patients. Based on these parameters, high MAP3K6 expression was found to be associated with a decrease in relapse-free survival ($p=0.0019$) with a hazard ratio of 0.84 (0.75-0.84) (Figure 1).

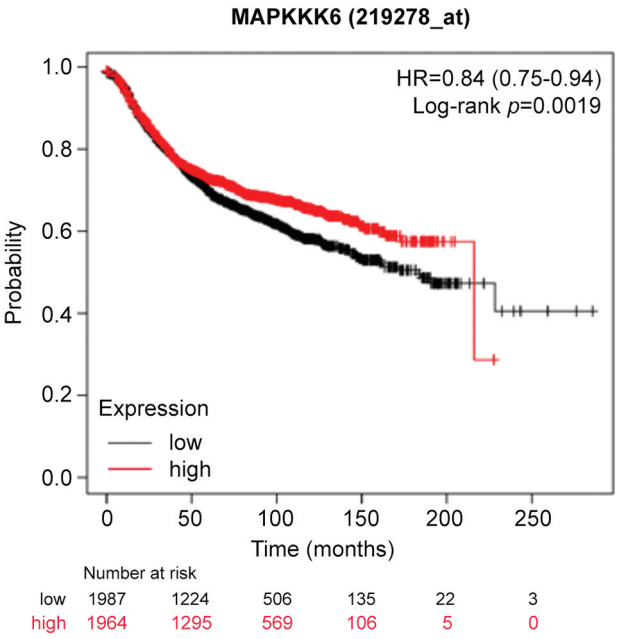

Figure 1. *High MAP3K6 expression is associated with decreased relapse-free survival in breast cancer patients. Using Kaplan–Meier Plotter (KM Plotter), publicly available microarray repositories for breast cancer were interrogated to determine whether MAP3K6 expression was associated with different survival rates among breast cancer patients. Hazard ratio (HR) and Log-rank p-values are shown. Low expression (below median) is noted in black, and the high expression (above median) is noted in red.*

The MAPK signaling cascade is activated as cells acquire resistance to letrozole. Since M3K6 exhibited the highest increase in expression between the two cell lines, we were interested in determining whether this alteration was associated with activation of the MAPK signaling cascades as a result of ER+ letrozole resistance. To study multiple proteins within this pathway and other receptor tyrosine kinase signaling cascades, the MAPK and RTK phospho-antibody arrays were utilized to measure the activation of key signaling components between the T47Darom and the T47DaromLR cells. We chose both arrays because a previous finding from our group demonstrated that HER2 expression was increased in the T47DaromLR cells (6). Although total HER2 expression was previously shown to be increased, activated ErbB2 (HER2) levels were decreased by 1.40-fold ($p<0.05$), suggesting this may not be a critical driver associated with ER+ AI resistance (Figure 2). We also observed increased expression of IGF1R which was previously found up-regulated in the LTLT-Ca cells (7).

When signaling components associated with the MAPK pathway were assessed, several phosphorylated proteins of interest were significantly increased including MKK6 (1.20-fold), p38 (1.41-fold), p70S6K (1.74-fold), phospho-Ribosomal S6 Kinase 1 (1.71-fold) and phospho-Ribosomal S6 Kinase 2 (4.74-fold) (Figure 3). This was highly relevant as this pathway is associated with growth, differentiation, apoptosis, and survival. Since there was not a significant change in Akt and mTOR expression, it is unlikely that the PI3K/Akt/mTOR pathway plays a major role in ER+ acquired AI resistance. Additionally, since both MEK and ERK1 were significantly decreased by 1.43- and 1.08-fold respectively, the Ras pathway may not be relevant. Taken together, this data suggests the p38/MAPK pathway may be a major driver of ER+ letrozole resistance. It was also noted that there was a 1.43-fold increase in p53 expression. This finding was not unusual as the T47D cell line expresses mutant p53 and in cultured cells, overexpression of tumor-associated p53 mutants has been shown to interfere with stress-induced apoptosis, increase resistance to chemotherapeutic drugs (8-12), promote genomic instability (13), and enhance proliferation (14).

The p38/MAPK pathway drives letrozole resistance. Since the proteomic analysis and the antibody array results demonstrated that increased p38/MAPK signaling was associated with the T47DaromLR cells, we wanted to determine whether inhibition of this pathway was responsible, in part, for the refractory nature of the cells as well as their aggressive phenotype. To test this, both the T47Darom and T47DaromLR cells were treated with 30 μM SB 203580 (a selective p38 MAPK) and proliferation was measured. Our results demonstrated that while the T47Darom cells were unaffected by SB 203580 treatment,

Table I. *Up-regulated proteins in letrozole resistant T47DaromLR breast cancer cells. Proteomic analyses were performed as described in the Methods section and the ratio of the fold change in T47DaromLR/T47Darom cells is shown. Text in bold indicates the proteins exhibiting the greatest fold change.*

Accession	Description	# AAs	MW [kDa]	Fold change	*t*-test (*p*-Value)
O95382	**Mitogen-activated protein kinase 6 OS=Homo sapiens GN=MAP3K6 PE=1 SV=3 - [M3K6_HUMAN]**	**1,288**	**142.506**	**3.2037514**	$p<0.01$
H0Y3Z3	**Protein disulfide-isomerase (Fragment) OS=Homo sapiens GN=P4HB PE=1 SV=1 - [H0Y3Z3_HUMAN]**	**274**	**31.5234**	**3.1950322**	$p<0.01$
Q9NU22	**Midasin OS=Homo sapiens GN=MDN1 PE=1 SV=2 - [MDN1_HUMAN]**	**5,596**	**632.42**	**2.7587754**	$p<0.001$
R4GN98	Protein S100 (Fragment) OS=Homo sapiens GN=S100A6 PE=1 SV=1 - [R4GN98_HUMAN]	85	9.67506	2.6447744	$p<0.01$
P60903	Protein S100-A10 OS=Homo sapiens GN=S100A10 PE=1 SV=2 - [S10AA_HUMAN]	97	11.1955	2.5544666	$p<0.001$
K7EQI0	Paragranulin (Fragment) OS=Homo sapiens GN=GRN PE=4 SV=1 - [K7EQI0_HUMAN]	110	11.8242	2.4237794	$p<0.01$
P04083	Annexin A1 OS=Homo sapiens GN=ANXA1 PE=1 SV=2 - [ANXA1_HUMAN]	346	38.69	2.1587977	$p<0.001$
E5RG29	Aspartyl/asparaginyl beta-hydroxylase (Fragment) OS=Homo sapiens GN=ASPH PE=4 SV=1 - [E5RG29_HUMAN]	198	22.2265	2.1382553	$p<0.01$
H0YA55	Serum albumin (Fragment) OS=Homo sapiens GN=ALB PE=1 SV=1 - [H0YA55_HUMAN]	454	51.5358	2.129391	$p<0.001$
A0A087WYQ7	Kynureninase (Fragment) OS=Homo sapiens GN=KYNU PE=1 SV=1 - [A0A087WYQ7_HUMAN]	157	17.3711	2.0269261	$p<0.05$
P07476	Involucrin OS=Homo sapiens GN=IVL PE=1 SV=2 - [INVO_HUMAN]	585	68.4372	1.9934225	$p<0.01$
F5H7F6	Microsomal glutathione S-transferase 1 (Fragment) OS=Homo sapiens GN=MGST1 PE=1 SV=1 - [F5H7F6_HUMAN]	77	8.88048	1.8163795	$p<0.001$
Q9P2D1	Chromodomain-helicase-DNA-binding protein 7 OS=Homo sapiens GN=CHD7 PE=1 SV=3 - [CHD7_HUMAN]	2,997	335.717	1.8045951	$p<0.01$
O76070	Gamma-synuclein OS=Homo sapiens GN=SNCG PE=1 SV=2 - [SYUG_HUMAN]	127	13.3228	1.7970365	$p<0.001$
P07355	Annexin A2 OS=Homo sapiens GN=ANXA2 PE=1 SV=2 - [ANXA2_HUMAN]	339	38.5798	1.7904175	$p<0.001$
E9PKU7	Neutral alpha-glucosidase AB OS=Homo sapiens GN=GANAB PE=1 SV=1 - [E9PKU7_HUMAN]	852	96.4831	1.7543555	$p<0.001$
P31949	Protein S100-A11 OS=Homo sapiens GN=S100A11 PE=1 SV=2 - [S10AB_HUMAN]	105	11.7328	1.7525625	$p<0.01$
P08729	Keratin, type II cytoskeletal 7 OS=Homo sapiens GN=KRT7 PE=1 SV=5 - [K2C7_HUMAN]	469	51.3543	1.7525381	$p<0.001$
Q14019	Coactosin-like protein OS=Homo sapiens GN=COTL1 PE=1 SV=3 - [COTL1_HUMAN]	142	15.935	1.7007204	$p<0.001$
A0A087WUZ6	InaD-like protein OS=Homo sapiens GN=INADL PE=1 SV=1 - [A0A087WUZ6_HUMAN]	1,182	130	1.6896547	$p<0.001$
P50897	Palmitoyl-protein thioesterase 1 OS=Homo sapiens GN=PPT1 PE=1 SV=1 - [PPT1_HUMAN]	306	34.1713	1.6864107	$p<0.001$
R4GN18	Membrane cofactor protein (Fragment) OS=Homo sapiens GN=CD46 PE=4 SV=1 - [R4GN18_HUMAN]	78	8.4965	1.636669	$p<0.001$
P02647	Apolipoprotein A-I OS=Homo sapiens GN=APOA1 PE=1 SV=1 - [APOA1_HUMAN]	267	30.7589	1.624178	$p<0.001$
Q8WWA1	Transmembrane protein 40 OS=Homo sapiens GN=TMEM40 PE=1 SV=2 - [TMM40_HUMAN]	233	25.4793	1.6170389	$p<0.001$
P09467	Fructose-1,6-bisphosphatase 1 OS=Homo sapiens GN=FBP1 PE=1 SV=5 - [F16P1_HUMAN]	338	36.8188	1.6147259	$p<0.001$
Q15847	Adipogenesis regulatory factor OS=Homo sapiens GN=ADIRF PE=1 SV=1 - [ADIRF_HUMAN]	76	7.84997	1.6089368	$p<0.01$
O76062	Delta(14)-sterol reductase OS=Homo sapiens GN=TM7SF2 PE=2 SV=3 - [ERG24_HUMAN]	418	46.3755	1.608441	$p<0.001$
P05026	Sodium/potassium-transporting ATPase subunit beta-1 OS=Homo sapiens GN=ATP1B1 PE=1 SV=1 - [AT1B1_HUMAN]	303	35.0389	1.6033027	$p<0.001$

Table I. *Continued*

Table I. *Continued*

Accession	Description	# AAs	MW [kDa]	Fold change	*t*-test (*p*-Value)
P12532	Creatine kinase U-type, mitochondrial OS=Homo sapiens GN=CKMT1A PE=1 SV=1 - [KCRU_HUMAN]	417	47.0072	1.595103	$p<0.001$
P02533	Keratin, type I cytoskeletal 14 OS=Homo sapiens GN=KRT14 PE=1 SV=4 - [K1C14_HUMAN]	472	51.5294	1.5900658	$p<0.01$
F5H2R5	Rho GDP-dissociation inhibitor 2 (Fragment) OS=Homo sapiens GN=ARHGDIB PE=1 SV=1 - [F5H2R5_HUMAN]	88	9.78591	1.5776326	$p<0.001$
P30038	Delta-1-pyrroline-5-carboxylate dehydrogenase, mitochondrial OS=Homo sapiens GN=ALDH4A1 PE=1 SV=3 - [AL4A1_HUMAN]	563	61.6806	1.5699616	$p<0.001$
J3KQ45	Trans-Golgi network integral membrane protein 2 OS=Homo sapiens GN=TGOLN2 PE=1 SV=1 - [J3KQ45_HUMAN]	454	47.8517	1.5653502	$p<0.001$
Q96C23	Aldose 1-epimerase OS=Homo sapiens GN=GALM PE=1 SV=1 - [GALM_HUMAN]	342	37.7421	1.5599502	$p<0.001$
O15173	Membrane-associated progesterone receptor component 2 OS=Homo sapiens GN=PGRMC2 PE=1 SV=1 - [PGRC2_HUMAN]	223	23.8037	1.5508404	$p<0.001$
P14406	Cytochrome c oxidase subunit 7A2, mitochondrial OS=Homo sapiens GN=COX7A2 PE=1 SV=1 - [CX7A2_HUMAN]	83	9.39011	1.5499904	$p<0.001$
F5GYS3	Bcl2-associated agonist of cell death OS=Homo sapiens GN=BAD PE=1 SV=1 - [F5GYS3_HUMAN]	157	16.6392	1.5392774	$p<0.01$
Q13011	Delta(3,5)-Delta(2,4)-dienoyl-CoA isomerase, mitochondrial OS=Homo sapiens GN=ECH1 PE=1 SV=2 - [ECH1_HUMAN]	328	35.7934	1.5385737	$p<0.01$
P05091	Aldehyde dehydrogenase, mitochondrial OS=Homo sapiens GN=ALDH2 PE=1 SV=2 - [ALDH2_HUMAN]	517	56.3456	1.5385587	$p<0.001$
Q5JQF8	Polyadenylate-binding protein 1-like 2 OS=Homo sapiens GN=PABPC1L2A PE=2 SV=1 - [PAP1M_HUMAN]	200	22.7846	1.5341699	$p<0.001$
I3L0Y5	ATP synthase F(0) complex subunit C1, mitochondrial (Fragment) OS=Homo sapiens GN=ATP5G1 PE=3 SV=1 - [I3L0Y5_HUMAN]	98	10.0322	1.5333557	$p<0.05$
K7EKD8	Calpain small subunit 1 OS=Homo sapiens GN=CAPNS1 PE=1 SV=1 - [K7EKD8_HUMAN]	238	24.786	1.5273755	$p<0.001$
P25815	Protein S100-P OS=Homo sapiens GN=S100P PE=1 SV=2 - [S100P_HUMAN]	95	10.3932	1.4987172	$p<0.01$
E9PB18	UPF0577 protein KIAA1324 (Fragment) OS=Homo sapiens GN=KIAA1324 PE=4 SV=1 - [E9PB18_HUMAN]	901	99.3015	1.4958927	$p<0.001$
P07237	Protein disulfide-isomerase OS=Homo sapiens GN=P4HB PE=1 SV=3 - [PDIA1_HUMAN]	508	57.0807	1.4837204	$p<0.001$
Q9UHB6	LIM domain and actin-binding protein 1 OS=Homo sapiens GN=LIMA1 PE=1 SV=1 - [LIMA1_HUMAN]	759	85.1734	1.4787853	$p<0.001$
P18463	HLA class I histocompatibility antigen, B-37 alpha chain OS=Homo sapiens GN=HLA-B PE=1 SV=1 - [1B37_HUMAN]	362	40.4311	1.4620279	$p<0.001$
A0A087WT15	Putative bifunctional UDP-N-acetylglucosamine transferase and deubiquitinase ALG13 OS=Homo sapiens GN=ALG13 PE=4 SV=1 - [A0A087WT15_HUMAN]	61	6.87346	1.4589875	$p<0.01$
P40121	Macrophage-capping protein OS=Homo sapiens GN=CAPG PE=1 SV=2 - [CAPG_HUMAN]	348	38.4745	1.4573444	$p<0.001$
Q9Y2Q3	Glutathione S-transferase kappa 1 OS=Homo sapiens GN=GSTK1 PE=1 SV=3 - [GSTK1_HUMAN]	226	25.4803	1.4570236	$p<0.001$
P04062	Glucosylceramidase OS=Homo sapiens GN=GBA PE=1 SV=3 - [GLCM_HUMAN]	536	59.6782	1.4367309	$p<0.001$
Q9UBM7	7-dehydrocholesterol reductase OS=Homo sapiens GN=DHCR7 PE=1 SV=1 - [DHCR7_HUMAN]	475	54.4538	1.4332229	$p<0.001$
Q9Y6N5	Sulfide:quinone oxidoreductase, mitochondrial OS=Homo sapiens GN=SQRDL PE=1 SV=1 - [SQRD_HUMAN]	450	49.9289	1.4319068	$p<0.001$
P00367	Glutamate dehydrogenase 1, mitochondrial OS=Homo sapiens GN=GLUD1 PE=1 SV=2 - [DHE3_HUMAN]	558	61.3592	1.4305508	$p<0.001$
O95716	Ras-related protein Rab-3D OS=Homo sapiens GN=RAB3D PE=1 SV=1 - [RAB3D_HUMAN]	219	24.2518	1.4262913	$p<0.001$
Q24JP5	Transmembrane protein 132A OS=Homo sapiens GN=TMEM132A PE=2 SV=1 - [T132A_HUMAN]	1,023	110.041	1.4186958	$p<0.001$
D6RA82	Annexin OS=Homo sapiens GN=ANXA3 PE=1 SV=1 - [D6RA82_HUMAN]	284	32.0985	1.4022738	$p<0.001$

Table I. *Continued*

Table I. *Continued*

Accession	Description	# AAs	MW [kDa]	Fold change	*t*-test (*p*-Value)
P53007	Tricarboxylate transport protein, mitochondrial OS=Homo sapiens GN=SLC25A1 PE=1 SV=2 - [TXTP_HUMAN]	311	33.991	1.3987563	$p<0.001$
Q8TE77	Protein phosphatase Slingshot homolog 3 OS=Homo sapiens GN=SSH3 PE=1 SV=2 - [SSH3_HUMAN]	659	72.9505	1.3976351	$p<0.001$
Q10589	Bone marrow stromal antigen 2 OS=Homo sapiens GN=BST2 PE=1 SV=1 - [BST2_HUMAN]	180	19.7563	1.3894274	$p<0.001$
F8VV56	CD63 antigen OS=Homo sapiens GN=CD63 PE=1 SV=1 - [F8VV56_HUMAN]	145	16.0099	1.3848263	$p<0.05$
Q14165	Malectin OS=Homo sapiens GN=MLEC PE=1 SV=1 - [MLEC_HUMAN]	292	32.2136	1.3751279	$p<0.001$
A3KMH1	von Willebrand factor A domain-containing protein 8 OS=Homo sapiens GN=VWA8 PE=1 SV=2 - [VWA8_HUMAN]	1,905	214.689	1.3749854	$p<0.01$
P10606	Cytochrome c oxidase subunit 5B, mitochondrial OS=Homo sapiens GN=COX5B PE=1 SV=2 - [COX5B_HUMAN]	129	13.6869	1.3698091	$p<0.01$
A0A087WVJ0	Mucin-1 (Fragment) OS=Homo sapiens GN=MUC1 PE=4 SV=1 - [A0A087WVJ0_HUMAN]	228	25.5498	1.3697826	$p<0.001$
Q9Y3Q3	Transmembrane emp24 domain-containing protein 3 OS=Homo sapiens GN=TMED3 PE=1 SV=1 - [TMED3_HUMAN]	217	24.7613	1.3645039	$p<0.01$
P07686	Beta-hexosaminidase subunit beta OS=Homo sapiens GN=HEXB PE=1 SV=3 - [HEXB_HUMAN]	556	63.0712	1.3635416	$p<0.001$
O95816	BAG family molecular chaperone regulator 2 OS=Homo sapiens GN=BAG2 PE=1 SV=1 - [BAG2_HUMAN]	211	23.7572	1.3633407	$p<0.01$
P09525	Annexin A4 OS=Homo sapiens GN=ANXA4 PE=1 SV=4 - [ANXA4_HUMAN]	319	35.8601	1.3605119	$p<0.001$
Q9Y394	Dehydrogenase/reductase SDR family member 7 OS=Homo sapiens GN=DHRS7 PE=1 SV=1 - [DHRS7_HUMAN]	339	38.2741	1.3556808	$p<0.001$
P58107	Epiplakin OS=Homo sapiens GN=EPPK1 PE=1 SV=2 - [EPIPL_HUMAN]	5,090	555.279	1.3520266	$p<0.001$
P00491	Purine nucleoside phosphorylase OS=Homo sapiens GN=PNP PE=1 SV=2 - [PNPH_HUMAN]	289	32.0972	1.3504636	$p<0.001$
O00625	Pirin OS=Homo sapiens GN=PIR PE=1 SV=1 - [PIR_HUMAN]	290	32.0933	1.3476629	$p<0.01$
Q9BVC6	Transmembrane protein 109 OS=Homo sapiens GN=TMEM109 PE=1 SV=1 - [TM109_HUMAN]	243	26.1936	1.343218	$p<0.001$
Q9NR28	Diablo homolog, mitochondrial OS=Homo sapiens GN=DIABLO PE=1 SV=1 - [DBLOH_HUMAN]	239	27.1137	1.3408889	$p<0.01$
Q86UP2	Kinectin OS=Homo sapiens GN=KTN1 PE=1 SV=1 - [KTN1_HUMAN]	1,357	156.179	1.3392072	$p<0.001$
P04181	Ornithine aminotransferase, mitochondrial OS=Homo sapiens GN=OAT PE=1 SV=1 - [OAT_HUMAN]	439	48.5042	1.3330075	$p<0.001$
O15270	Serine palmitoyltransferase 2 OS=Homo sapiens GN=SPTLC2 PE=1 SV=1 - [SPTC2_HUMAN]	562	62.8839	1.3326487	$p<0.05$
E9PF16	Acyl-CoA synthetase family member 2, mitochondrial OS=Homo sapiens GN=ACSF2 PE=4 SV=1 - [E9PF16_HUMAN]	572	63.6114	1.3315351	$p<0.01$
Q14956	Transmembrane glycoprotein NMB OS=Homo sapiens GN=GPNMB PE=1 SV=2 - [GPNMB_HUMAN]	572	63.8819	1.3315248	$p<0.01$
O75531	Barrier-to-autointegration factor OS=Homo sapiens GN=BANF1 PE=1 SV=1 - [BAF_HUMAN]	89	10.052	1.3302003	$p<0.01$
Q9H0U4	Ras-related protein Rab-1B OS=Homo sapiens GN=RAB1B PE=1 SV=1 - [RAB1B_HUMAN]	201	22.1572	1.3258098	$p<0.001$
P05783	Keratin, type I cytoskeletal 18 OS=Homo sapiens GN=KRT18 PE=1 SV=2 - [K1C18_HUMAN]	430	48.0285	1.3239039	$p<0.001$
Q9UDW1	Cytochrome b-c1 complex subunit 9 OS=Homo sapiens GN=UQCR10 PE=1 SV=3 - [QCR9_HUMAN]	63	7.30383	1.3232184	$p<0.001$
H3BM67	Nucleolar protein 3 (Fragment) OS=Homo sapiens GN=NOL3 PE=4 SV=3 - [H3BM67_HUMAN]	139	15.0125	1.3207562	$p<0.01$
P50454	Serpin H1 OS=Homo sapiens GN=SERPINH1 PE=1 SV=2 - [SERPH_HUMAN]	418	46.4112	1.3189995	$p<0.001$
P15529	Membrane cofactor protein OS=Homo sapiens GN=CD46 PE=1 SV=3 - [MCP_HUMAN]	392	43.7187	1.3184128	$p<0.01$

Table I. *Continued*

Table I. *Continued*

Accession	Description	# AAs	MW [kDa]	Fold change	*t*-test (*p*-Value)
J3KT68	Transmembrane protein 97 OS=Homo sapiens GN=TMEM97 PE=1 SV=1 - [J3KT68_HUMAN]	92	10.9688	1.3162762	$p<0.01$
P35232	Prohibitin OS=Homo sapiens GN=PHB PE=1 SV=1 - [PHB_HUMAN]	272	29.7859	1.3155472	$p<0.001$
P29373	Cellular retinoic acid-binding protein 2 OS=Homo sapiens GN=CRABP2 PE=1 SV=2 - [RABP2_HUMAN]	138	15.683	1.3147	$p<0.001$
Q9BR76	Coronin-1B OS=Homo sapiens GN=CORO1B PE=1 SV=1 - [COR1B_HUMAN]	489	54.2003	1.3079348	$p<0.001$
P61604	10 kDa heat shock protein, mitochondrial OS=Homo sapiens GN=HSPE1 PE=1 SV=2 - [CH10_HUMAN]	102	10.9249	1.3066874	$p<0.01$
P14314	Glucosidase 2 subunit beta OS=Homo sapiens GN=PRKCSH PE=1 SV=2 - [GLU2B_HUMAN]	528	59.3878	1.3050784	$p<0.001$
H0YDJ4	Ninein (Fragment) OS=Homo sapiens GN=NIN PE=1 SV=1 - [H0YDJ4_HUMAN]	1,537	179.439	1.3034976	$p<0.01$
E7ERY9	Calcium-transporting ATPase OS=Homo sapiens GN=ATP2B1 PE=1 SV=2 - [E7ERY9_HUMAN]	963	106.789	1.30286	$p<0.001$
P26885	Peptidyl-prolyl cis-trans isomerase FKBP2 OS=Homo sapiens GN=FKBP2 PE=1 SV=2 - [FKBP2_HUMAN]	142	15.6393	1.3022129	$p<0.001$
Q9BTV4	Transmembrane protein 43 OS=Homo sapiens GN=TMEM43 PE=1 SV=1 - [TMM43_HUMAN]	400	44.8472	1.3012834	$p<0.001$
Q15075	Early endosome antigen 1 OS=Homo sapiens GN=EEA1 PE=1 SV=2 - [EEA1_HUMAN]	1,411	162.367	1.2999296	$p<0.001$
P04004	Vitronectin OS=Homo sapiens GN=VTN PE=1 SV=1 - [VTNC_HUMAN]	478	54.2712	1.2952339	$p<0.001$
Q6P996	Pyridoxal-dependent decarboxylase domain-containing protein 1 OS=Homo sapiens GN=PDXDC1 PE=1 SV=2 - [PDXD1_HUMAN]	788	86.6523	1.2938765	$p<0.05$
P04179	Superoxide dismutase [Mn], mitochondrial OS=Homo sapiens GN=SOD2 PE=1 SV=2 - [SODM_HUMAN]	222	24.7066	1.293093	$p<0.001$
M0QYZ0	Heterogeneous nuclear ribonucleoprotein U-like protein 1 (Fragment) OS=Homo sapiens GN=HNRNPUL1 PE=1 SV=1 - [M0QYZ0_HUMAN]	371	42.2697	1.2927079	$p<0.001$
Q9BZQ8	Protein Niban OS=Homo sapiens GN=FAM129A PE=1 SV=1 - [NIBAN_HUMAN]	928	103.07	1.2916002	$p<0.001$
P00390	Glutathione reductase, mitochondrial OS=Homo sapiens GN=GSR PE=1 SV=2 - [GSHR_HUMAN]	522	56.221	1.290853	$p<0.001$
K7EM09	Transmembrane protein 205 (Fragment) OS=Homo sapiens GN=TMEM205 PE=1 SV=1 - [K7EM09_HUMAN]	120	13.3807	1.2885968	$p<0.001$
I3L3E4	Charged multivesicular body protein 6 (Fragment) OS=Homo sapiens GN=CHMP6 PE=1 SV=1 - [I3L3E4_HUMAN]	113	12.9314	1.2840595	$p<0.05$
Q9BX68	Histidine triad nucleotide-binding protein 2, mitochondrial OS=Homo sapiens GN=HINT2 PE=1 SV=1 - [HINT2_HUMAN]	163	17.1512	1.2837525	$p<0.001$
P45973	Chromobox protein homolog 5 OS=Homo sapiens GN=CBX5 PE=1 SV=1 - [CBX5_HUMAN]	191	22.2111	1.281572	$p<0.001$
P05787	Keratin, type II cytoskeletal 8 OS=Homo sapiens GN=KRT8 PE=1 SV=7 - [K2C8_HUMAN]	483	53.6711	1.2780591	$p<0.001$
H0Y339	E3 ubiquitin-protein ligase RFWD2 (Fragment) OS=Homo sapiens GN=RFWD2 PE=4 SV=1 - [H0Y339_HUMAN]	566	64.4877	1.2775849	$p<0.01$
P02787	Serotransferrin OS=Homo sapiens GN=TF PE=1 SV=3 - [TRFE_HUMAN]	698	77.0136	1.2759193	$p<0.01$
A8MT65	Zinc finger protein 891 OS=Homo sapiens GN=ZNF891 PE=2 SV=2 - [ZN891_HUMAN]	544	63.5502	1.2734141	$p<0.01$
O75874	Isocitrate dehydrogenase [NADP] cytoplasmic OS=Homo sapiens GN=IDH1 PE=1 SV=2 - [IDHC_HUMAN]	414	46.6295	1.2724354	$p<0.001$
P12236	ADP/ATP translocase 3 OS=Homo sapiens GN=SLC25A6 PE=1 SV=4 - [ADT3_HUMAN]	298	32.8452	1.2713881	$p<0.01$
O75131	Copine-3 OS=Homo sapiens GN=CPNE3 PE=1 SV=1 - [CPNE3_HUMAN]	537	60.0921	1.2713204	$p<0.001$
F8VVM2	Phosphate carrier protein, mitochondrial OS=Homo sapiens GN=SLC25A3 PE=1 SV=1 - [F8VVM2_HUMAN]	324	36.1376	1.2702845	$p<0.001$

Table I. *Continued*

Table I. *Continued*

Accession	Description	# AAs	MW [kDa]	Fold change	*t*-test (*p*-Value)
Q2TAY7	WD40 repeat-containing protein SMU1 OS=Homo sapiens GN=SMU1 PE=1 SV=2 - [SMU1_HUMAN]	513	57.5072	1.2690306	$p<0.001$
Q15293	Reticulocalbin-1 OS=Homo sapiens GN=RCN1 PE=1 SV=1 - [RCN1_HUMAN]	331	38.8662	1.2635162	$p<0.001$
E9PM95	Apolipoprotein L2 (Fragment) OS=Homo sapiens GN=APOL2 PE=1 SV=1 - [E9PM95_HUMAN]	128	14.9386	1.2630585	$p<0.01$
A0A087X208	Agrin OS=Homo sapiens GN=AGRN PE=4 SV=1 - [A0A087X208_HUMAN]	1,930	202.162	1.2620734	$p<0.001$
A0A087WY61	Nuclear mitotic apparatus protein 1 OS=Homo sapiens GN=NUMA1 PE=1 SV=1 - [A0A087WY61_HUMAN]	2,099	236.019	1.2614504	$p<0.001$
Q16698	2,4-dienoyl-CoA reductase, mitochondrial OS=Homo sapiens GN=DECR1 PE=1 SV=1 - [DECR_HUMAN]	335	36.0448	1.2589002	$p<0.001$
Q14011	Cold-inducible RNA-binding protein OS=Homo sapiens GN=CIRBP PE=1 SV=1 - [CIRBP_HUMAN]	172	18.6367	1.2565207	$p<0.001$
P14625	Endoplasmin OS=Homo sapiens GN=HSP90B1 PE=1 SV=1 - [ENPL_HUMAN]	803	92.4113	1.2542374	$p<0.001$
Q96HE7	ERO1-like protein alpha OS=Homo sapiens GN=ERO1L PE=1 SV=2 - [ERO1A_HUMAN]	468	54.3581	1.2516932	$p<0.001$
P17900	Ganglioside GM2 activator OS=Homo sapiens GN=GM2A PE=1 SV=4 - [SAP3_HUMAN]	193	20.8247	1.2515007	$p<0.001$
P27824	Calnexin OS=Homo sapiens GN=CANX PE=1 SV=2 - [CALX_HUMAN]	592	67.5259	1.2502035	$p<0.001$

there was a 1.47-fold ($p<0.0001$) reduction in the proliferation of the T47DaromLR cells (Figure 4). As the growth of the T47DaromLR cells was selectively decreased by the p38 inhibitor, we chose to assess whether this effect was associated with alterations in apoptosis. The caspase 3/7 assay was performed on both cell lines in the presence and absence of the p38 inhibitor (Figure 5). While the T47Darom cells were unresponsive, there was a slight induction in apoptosis in the T47DaromLR cells treated with the p38 inhibitor, suggesting the p38/MAPK pathway may play a role in endocrine resistance.

Discussion

Aromatase inhibitors have been the first-line agents for post-menopausal women with hormone receptor positive metastatic breast cancer for many years. However, like many agents, some women develop resistance and stop responding to therapies, which can result in tumor relapse, metastasis, and a more aggressive phenotype. Thus, understanding mechanisms of resistance are critical to the development of novel strategies to address these patients. Previous reports by our group have identified a signature of letrozole resistance that was associated with estrogen independence, increased EGFR and HER2, enhanced motility, and an EMT phenotype (2). We focused on understanding the mechanisms of AI resistance associated with hormone refractory tumors, however the distinctions between AI-resistance in the hormone dependent versus hormone independent settings remain unclear.

Here, we utilized a non-migratory, ER+ letrozole resistant cell line (*i.e.*, derived from the T47D epithelial cells) as a model system to initially characterize changes that occur as cells transition to an acquired AI-resistant phenotype. Although these cells are ER+, they are cross resistant to the selective estrogen receptor modulator tamoxifen, (3) further demonstrating their aggressive nature and limited therapeutic options. As the AI-sensitive cells transitioned to AI-resistance, both HER2 and MAPK expression were induced (6). This was a similar phenomenon previously observed in the hormone-independent AI-resistant LTLT-Ca cells (2). When the protein expression of a panel of phosphorylated receptor tyrosine kinases were evaluated, pErbB2 (*i.e.*, pHER2) expression was decreased in the T47DaromLR cells compared to the T47DaromLR cells, suggesting that other pathways may be responsible for the acquired resistance. This was a unique feature of the T47DaromLR cells compared to the LTLT-Ca cells. Previous reports have demonstrated that increased pHER2 expression in the LTLT-Ca cells and trastuzumab was capable of reversing the resistance and restoring sensitivity to letrozole (15).

Since the T47DaromLR cells exhibited increased MAPK, we evaluated a panel of phosphorylated proteins involved in the MAPK signaling cascade. Signaling components and effectors of the p38/MAPK pathway (*i.e.*, MKK6 and p38)

Table II. *Down-regulated proteins in letrozole resistant T47DaromLR breast cancer cells. Proteomic analyses were performed as described in the Methods section and the ratio of the fold change in T47DaromLR/T47Darom cells is shown. The text in bold indicates a protein of interest.*

Accession	Description	# AAs	MW [kDa]	Fold change	*t*-test (*p*-value)
Q15185	Prostaglandin E synthase 3 OS=Homo sapiens GN=PTGES3 PE=1 SV=1 - [TEBP_HUMAN]	160	18.6854194	0.79904589	$p<0.01$
Q9NYL9	Tropomodulin-3 OS=Homo sapiens GN=TMOD3 PE=1 SV=1 - [TMOD3_HUMAN]	352	39.5703018	0.79902558	$p<0.05$
P18669	Phosphoglycerate mutase 1 OS=Homo sapiens GN=PGAM1 PE=1 SV=2 - [PGAM1_HUMAN]	254	28.7858365	0.79865701	$p<0.001$
P19338	Nucleolin OS=Homo sapiens GN=NCL PE=1 SV=3 - [NUCL_HUMAN]	710	76.5683628	0.79790721	$p<0.001$
Q12931	Heat shock protein 75 kDa, mitochondrial OS=Homo sapiens GN=TRAP1 PE=1 SV=3 - [TRAP1_HUMAN]	704	80.0596949	0.79777903	$p<0.001$
Q86Y56	HEAT repeat-containing protein 2 OS=Homo sapiens GN=HEATR2 PE=1 SV=4 - [HEAT2_HUMAN]	855	93.4620686	0.79675307	$p<0.001$
K7EJE8	Lon protease homolog, mitochondrial OS=Homo sapiens GN=LONP1 PE=1 SV=1 - [K7EJE8_HUMAN]	829	93.2379667	0.79656905	$p<0.001$
Q8IZ52	Chondroitin sulfate synthase 2 OS=Homo sapiens GN=CHPF PE=1 SV=2 - [CHSS2_HUMAN]	775	85.4140471	0.79611883	$p<0.01$
P31939	Bifunctional purine biosynthesis protein PURH OS=Homo sapiens GN=ATIC PE=1 SV=3 - [PUR9_HUMAN]	592	64.5753451	0.79607097	$p<0.001$
O15371	Eukaryotic translation initiation factor 3 subunit D OS=Homo sapiens GN=EIF3D PE=1 SV=1 - [EIF3D_HUMAN]	548	63.9324345	0.79584502	$p<0.001$
P12004	Proliferating cell nuclear antigen OS=Homo sapiens GN=PCNA PE=1 SV=1 - [PCNA_HUMAN]	261	28.7502945	0.79483268	$p<0.001$
P68371	Tubulin beta-4B chain OS=Homo sapiens GN=TUBB4B PE=1 SV=1 - [TBB4B_HUMAN]	445	49.7990043	0.79464307	$p<0.01$
V9GYX7	Actin-related protein 10 (Fragment) OS=Homo sapiens GN=ACTR10 PE=1 SV=1 - [V9GYX7_HUMAN]	302	33.2901748	0.79372567	$p<0.05$
P62258	14-3-3 protein epsilon OS=Homo sapiens GN=YWHAE PE=1 SV=1 - [1433E_HUMAN]	255	29.1554174	0.7932199	$p<0.001$
Q9NZL9	Methionine adenosyltransferase 2 subunit beta OS=Homo sapiens GN=MAT2B PE=1 SV=1 - [MAT2B_HUMAN]	334	37.5281776	0.7926943	$p<0.001$
P13995	Bifunctional methylenetetrahydrofolate dehydrogenase/ cyclohydrolase, mitochondrial OS=Homo sapiens GN=MTHFD2 PE=1 SV=2 - [MTDC_HUMAN]	350	37.8711975	0.79227913	$p<0.01$
P62826	GTP-binding nuclear protein Ran OS=Homo sapiens GN=RAN PE=1 SV=3 - [RAN_HUMAN]	216	24.4076189	0.791804	$p<0.001$
P50990	T-complex protein 1 subunit theta OS=Homo sapiens GN=CCT8 PE=1 SV=4 - [TCPQ_HUMAN]	548	59.582509	0.78997166	$p<0.001$
M0R210	40S ribosomal protein S16 OS=Homo sapiens GN=RPS16 PE=1 SV=1 - [M0R210_HUMAN]	129	14.4099586	0.78837739	$p<0.001$
Q9NPH2	Inositol-3-phosphate synthase 1 OS=Homo sapiens GN=ISYNA1 PE=1 SV=1 - [INO1_HUMAN]	558	61.029104	0.78806023	$p<0.01$
Q32Q12	Nucleoside diphosphate kinase OS=Homo sapiens GN=NME1-NME2 PE=1 SV=1 - [Q32Q12_HUMAN]	292	32.6208685	0.78792838	$p<0.001$
P40937	Replication factor C subunit 5 OS=Homo sapiens GN=RFC5 PE=1 SV=1 - [RFC5_HUMAN]	340	38.4721873	0.78511694	$p<0.01$
D6RFM5	Succinate dehydrogenase [ubiquinone] flavoprotein subunit, mitochondrial OS=Homo sapiens GN=SDHA PE=1 SV=1 - [D6RFM5_HUMAN]	583	63.5266889	0.78479348	$p<0.001$
H7C3S9	COP9 signalosome complex subunit 8 (Fragment) OS=Homo sapiens GN=COPS8 PE=1 SV=1 - [H7C3S9_HUMAN]	83	9.03868894	0.78280605	$p<0.001$
Q99536	Synaptic vesicle membrane protein VAT-1 homolog OS=Homo sapiens GN=VAT1 PE=1 SV=2 - [VAT1_HUMAN]	393	41.8934194	0.78202386	$p<0.001$
Q9BUF5	Tubulin beta-6 chain OS=Homo sapiens GN=TUBB6 PE=1 SV=1 - [TBB6_HUMAN]	446	49.8250022	0.78081583	$p<0.05$
Q9Y2Z0	Suppressor of G2 allele of SKP1 homolog OS=Homo sapiens GN=SUGT1 PE=1 SV=3 - [SUGT1_HUMAN]	365	40.998492	0.78075718	$p<0.05$
E7EUH7	Pseudouridylate synthase 7 homolog OS=Homo sapiens GN=PUS7 PE=1 SV=1 - [E7EUH7_HUMAN]	448	50.5206902	0.78060885	$p<0.05$

Table II. *Continued*

Table II. *Continued*

Accession	Description	# AAs	MW [kDa]	Fold change	*t*-test (*p*-value)
Q13907	Isopentenyl-diphosphate Delta-isomerase 1 OS=Homo sapiens GN=IDI1 PE=1 SV=2 - [IDI1_HUMAN]	227	26.3024914	0.7785156	$p<0.001$
F8VXD2	Cyclin-dependent kinase 4 (Fragment) OS=Homo sapiens GN=CDK4 PE=1 SV=1 - [F8VXD2_HUMAN]	132	14.8906691	0.77756677	$p<0.05$
P08559	Pyruvate dehydrogenase E1 component subunit alpha, somatic form, mitochondrial OS=Homo sapiens GN=PDHA1 PE=1 SV=3 - [ODPA_HUMAN]	390	43.2676109	0.77727405	$p<0.001$
O00762	Ubiquitin-conjugating enzyme E2 C OS=Homo sapiens GN=UBE2C PE=1 SV=1 - [UBE2C_HUMAN]	179	19.6399202	0.77693257	$p<0.001$
P43490	Nicotinamide phosphoribosyltransferase OS=Homo sapiens GN=NAMPT PE=1 SV=1 - [NAMPT_HUMAN]	491	55.4865965	0.77652882	$p<0.001$
D6RDM7	Ubiquitin-conjugating enzyme E2 K (Fragment) OS=Homo sapiens GN=UBE2K PE=1 SV=1 - [D6RDM7_HUMAN]	123	14.0261903	0.77622448	$p<0.001$
E5RFP0	NudC domain-containing protein 2 OS=Homo sapiens GN=NUDCD2 PE=1 SV=1 - [E5RFP0_HUMAN]	132	14.7361652	0.77511218	$p<0.01$
Q04917	14-3-3 protein eta OS=Homo sapiens GN=YWHAH PE=1 SV=4 - [1433F_HUMAN]	246	28.20102	0.77478302	$p<0.01$
P29144	Tripeptidyl-peptidase 2 OS=Homo sapiens GN=TPP2 PE=1 SV=4 - [TPP2_HUMAN]	1,249	138.262632	0.77415019	$p<0.01$
P68032	Actin, alpha cardiac muscle 1 OS=Homo sapiens GN=ACTC1 PE=1 SV=1 - [ACTC_HUMAN]	377	41.9918826	0.77329561	$p<0.001$
Q562R1	Beta-actin-like protein 2 OS=Homo sapiens GN=ACTBL2 PE=1 SV=2 - [ACTBL_HUMAN]	376	41.9759693	0.76932533	$p<0.001$
Q14914	Prostaglandin reductase 1 OS=Homo sapiens GN=PTGR1 PE=1 SV=2 - [PTGR1_HUMAN]	329	35.8467307	0.76842181	$p<0.01$
Q05639	Elongation factor 1-alpha 2 OS=Homo sapiens GN=EEF1A2 PE=1 SV=1 - [EF1A2_HUMAN]	463	50.4383096	0.76649072	$p<0.001$
P06396	Gelsolin OS=Homo sapiens GN=GSN PE=1 SV=1 - [GELS_HUMAN]	782	85.6441934	0.76419352	$p<0.001$
P11908	Ribose-phosphate pyrophosphokinase 2 OS=Homo sapiens GN=PRPS2 PE=1 SV=2 - [PRPS2_HUMAN]	318	34.7469789	0.76381858	$p<0.01$
Q58FF6	Putative heat shock protein HSP 90-beta 4 OS=Homo sapiens GN=HSP90AB4P PE=5 SV=1 - [H90B4_HUMAN]	505	58.2275805	0.76277969	$p<0.001$
H7C3P9	COP9 signalosome complex subunit 3 OS=Homo sapiens GN=COPS3 PE=1 SV=2 - [H7C3P9_HUMAN]	345	39.0105281	0.76178683	$p<0.001$
P80404	4-aminobutyrate aminotransferase, mitochondrial OS=Homo sapiens GN=ABAT PE=1 SV=3 - [GABT_HUMAN]	500	56.4025903	0.75993164	$p<0.001$
P17174	Aspartate aminotransferase, cytoplasmic OS=Homo sapiens GN=GOT1 PE=1 SV=3 - [AATC_HUMAN]	413	46.2185309	0.75976861	$p<0.001$
Q9HB71	Calcyclin-binding protein OS=Homo sapiens GN=CACYBP PE=1 SV=2 - [CYBP_HUMAN]	228	26.1936459	0.75789333	$p<0.001$
P62328	Thymosin beta-4 OS=Homo sapiens GN=TMSB4X PE=1 SV=2 - [TYB4_HUMAN]	44	5.04951649	0.75606602	$p<0.05$
E9PNK6	Tumor protein D53 OS=Homo sapiens GN=TPD52L1 PE=1 SV=1 - [E9PNK6_HUMAN]	166	18.6492831	0.75524912	$p<0.01$
Q96IU4	Alpha/beta hydrolase domain-containing protein 14B OS=Homo sapiens GN=ABHD14B PE=1 SV=1 - [ABHEB_HUMAN]	210	22.3315574	0.75457008	$p<0.01$
Q9NP72	Ras-related protein Rab-18 OS=Homo sapiens GN=RAB18 PE=1 SV=1 - [RAB18_HUMAN]	206	22.9626389	0.7544287	$p<0.001$
C9JLU1	DNA-directed RNA polymerases I, II, and III subunit RPABC3 (Fragment) OS=Homo sapiens GN=POLR2H PE=1 SV=3 - [C9JLU1_HUMAN]	149	16.9853803	0.75427123	$p<0.01$
Q8N0Y7	Probable phosphoglycerate mutase 4 OS=Homo sapiens GN=PGAM4 PE=2 SV=1 - [PGAM4_HUMAN]	254	28.7587667	0.75337853	$p<0.05$
E9PLT0	Cold shock domain-containing protein E1 OS=Homo sapiens GN=CSDE1 PE=1 SV=1 - [E9PLT0_HUMAN]	668	74.5367585	0.75176491	$p<0.001$
P07900	Heat shock protein HSP 90-alpha OS=Homo sapiens GN=HSP90AA1 PE=1 SV=5 - [HS90A_HUMAN]	732	84.6066852	0.75149833	$p<0.001$

Table II. *Continued*

Table II. *Continued*

Accession	Description	# AAs	MW [kDa]	Fold change	*t*-test (*p*-value)
F5H345	Porphobilinogen deaminase OS=Homo sapiens GN=HMBS PE=1 SV=1 - [F5H345_HUMAN]	330	35.7388228	0.75086131	$p<0.01$
P41227	N-alpha-acetyltransferase 10 OS=Homo sapiens GN=NAA10 PE=1 SV=1 - [NAA10_HUMAN]	235	26.4418527	0.75055952	$p<0.001$
P35580	Myosin-10 OS=Homo sapiens GN=MYH10 PE=1 SV=3 - [MYH10_HUMAN]	1,976	228.857964	0.75001828	$p<0.01$
P36507	Dual specificity mitogen-activated protein kinase kinase 2 OS=Homo sapiens GN=MAP2K2 PE=1 SV=1 - [MP2K2_HUMAN]	400	44.396055	0.7484181	$p<0.01$
Q9UNF1	Melanoma-associated antigen D2 OS=Homo sapiens GN=MAGED2 PE=1 SV=2 - [MAGD2_HUMAN]	606	64.9143628	0.74753167	$p<0.001$
P61981	14-3-3 protein gamma OS=Homo sapiens GN=YWHAG PE=1 SV=2 - [1433G_HUMAN]	247	28.2849139	0.74714741	$p<0.001$
Q9Y265	RuvB-like 1 OS=Homo sapiens GN=RUVBL1 PE=1 SV=1 - [RUVB1_HUMAN]	456	50.1963165	0.74346671	$p<0.001$
Q7L2H7	Eukaryotic translation initiation factor 3 subunit M OS=Homo sapiens GN=EIF3M PE=1 SV=1 - [EIF3M_HUMAN]	374	42.475807	0.74293059	$p<0.01$
Q9BQE3	Tubulin alpha-1C chain OS=Homo sapiens GN=TUBA1C PE=1 SV=1 - [TBA1C_HUMAN]	449	49.8634645	0.74276939	$p<0.001$
P13639	Elongation factor 2 OS=Homo sapiens GN=EEF2 PE=1 SV=4 - [EF2_HUMAN]	858	95.2769538	0.73926002	$p<0.001$
C9JPA8	Golgi to ER traffic protein 4 homolog (Fragment) OS=Homo sapiens GN=GET4 PE=1 SV=2 - [C9JPA8_HUMAN]	148	16.5321422	0.73902176	$p<0.001$
Q53EL6	Programmed cell death protein 4 OS=Homo sapiens GN=PDCD4 PE=1 SV=2 - [PDCD4_HUMAN]	469	51.7030487	0.73378818	$p<0.001$
E5RG13	Inositol monophosphatase 1 (Fragment) OS=Homo sapiens GN=IMPA1 PE=1 SV=1 - [E5RG13_HUMAN]	153	17.0476334	0.73217864	$p<0.01$
O96019	Actin-like protein 6A OS=Homo sapiens GN=ACTL6A PE=1 SV=1 - [ACL6A_HUMAN]	429	47.4303444	0.7298752	$p<0.01$
O75369	Filamin-B OS=Homo sapiens GN=FLNB PE=1 SV=2 - [FLNB_HUMAN]	2,602	277.990071	0.72651996	$p<0.001$
P68363	Tubulin alpha-1B chain OS=Homo sapiens GN=TUBA1B PE=1 SV=1 - [TBA1B_HUMAN]	451	50.1196069	0.72651105	$p<0.001$
Q9H0C2	ADP/ATP translocase 4 OS=Homo sapiens GN=SLC25A31 PE=2 SV=1 - [ADT4_HUMAN]	315	34.9994373	0.72226342	$p<0.01$
Q8TC12	Retinol dehydrogenase 11 OS=Homo sapiens GN=RDH11 PE=1 SV=2 - [RDH11_HUMAN]	318	35.3634467	0.72142867	$p<0.001$
P08238	Heat shock protein HSP 90-beta OS=Homo sapiens GN=HSP90AB1 PE=1 SV=4 - [HS90B_HUMAN]	724	83.2121059	0.71815962	$p<0.001$
P11177	Pyruvate dehydrogenase E1 component subunit beta, mitochondrial OS=Homo sapiens GN=PDHB PE=1 SV=3 - [ODPB_HUMAN]	359	39.2080346	0.71532722	$p<0.001$
A0A087WWP8	Round spermatid basic protein 1 OS=Homo sapiens GN=RSBN1 PE=1 SV=1 - [A0A087WWP8_HUMAN]	754	84.922968	0.70870038	$p<0.05$
P00338	L-lactate dehydrogenase A chain OS=Homo sapiens GN=LDHA PE=1 SV=2 - [LDHA_HUMAN]	332	36.6653627	0.70859232	$p<0.001$
Q96CP2	FLYWCH family member 2 OS=Homo sapiens GN=FLYWCH2 PE=1 SV=1 - [FWCH2_HUMAN]	140	14.5545451	0.7042261	$p<0.05$
O00232	26S proteasome non-ATPase regulatory subunit 12 OS=Homo sapiens GN=PSMD12 PE=1 SV=3 - [PSD12_HUMAN]	456	52.8705755	0.70028253	$p<0.001$
P07437	Tubulin beta chain OS=Homo sapiens GN=TUBB PE=1 SV=2 - [TBB5_HUMAN]	444	49.6389736	0.69867551	$p<0.001$
Q9HAV0	Guanine nucleotide-binding protein subunit beta-4 OS=Homo sapiens GN=GNB4 PE=1 SV=3 - [GBB4_HUMAN]	340	37.5430236	0.69638699	$p<0.001$
P62937	Peptidyl-prolyl cis-trans isomerase A OS=Homo sapiens GN=PPIA PE=1 SV=2 - [PPIA_HUMAN]	165	18.0008862	0.69099459	$p<0.001$
P41250	Glycine--tRNA ligase OS=Homo sapiens GN=GARS PE=1 SV=3 - [SYG_HUMAN]	739	83.1126144	0.68820486	$p<0.001$
A0A087WW67	Inactive N-acetylated-alpha-linked acidic dipeptidase-like protein 2 OS=Homo sapiens GN=NAALADL2 PE=4 SV=1 - [A0A087WW67_HUMAN]	783	87.4024178	0.68607324	$p<0.01$

Table II. *Continued*

Table II. *Continued*

Accession	Description	# AAs	MW [kDa]	Fold change	*t*-test (*p*-value)
P52735	Guanine nucleotide exchange factor VAV2 OS=Homo sapiens GN=VAV2 PE=1 SV=2 - [VAV2_HUMAN]	878	101.223761	0.68510642	$p<0.001$
E9PCZ3	Type II inositol 3,4-bisphosphate 4-phosphatase (Fragment) OS=Homo sapiens GN=INPP4B PE=4 SV=1 - [E9PCZ3_HUMAN]	688	78.1047694	0.67949237	$p<0.001$
P09382	Galectin-1 OS=Homo sapiens GN=LGALS1 PE=1 SV=2 - [LEG1_HUMAN]	135	14.7062001	0.67748938	$p<0.001$
P48052	Carboxypeptidase A2 OS=Homo sapiens GN=CPA2 PE=1 SV=3 - [CBPA2_HUMAN]	419	47.0006266	0.67601541	$p<0.01$
K7ERE3	Keratin, type I cytoskeletal 13 OS=Homo sapiens GN=KRT13 PE=1 SV=1 - [K7ERE3_HUMAN]	415	45.232239	0.66812005	$p<0.001$
B3KUB4	Carbonic anhydrase 12 OS=Homo sapiens GN=CA12 PE=2 SV=1 - [B3KUB4_HUMAN]	283	31.8373497	0.66653472	$p<0.001$
Q5JVM0	Unconventional myosin-VI (Fragment) OS=Homo sapiens GN=MYO6 PE=1 SV=1 - [Q5JVM0_HUMAN]	174	20.5885602	0.66103342	$p<0.001$
Q13451	Peptidyl-prolyl cis-trans isomerase FKBP5 OS=Homo sapiens GN=FKBP5 PE=1 SV=2 - [FKBP5_HUMAN]	457	51.1795705	0.66044757	$p<0.001$
P21266	Glutathione S-transferase Mu 3 OS=Homo sapiens GN=GSTM3 PE=1 SV=3 - [GSTM3_HUMAN]	225	26.5421389	0.65763968	$p<0.001$
F5GWT4	Serine/threonine-protein kinase WNK1 OS=Homo sapiens GN=WNK1 PE=1 SV=1 - [F5GWT4_HUMAN]	2,134	225.364792	0.65376951	$p<0.01$
Q9BV86	N-terminal Xaa-Pro-Lys N-methyltransferase 1 OS=Homo sapiens GN=NTMT1 PE=1 SV=3 - [NTM1A_HUMAN]	223	25.3708399	0.65311967	$p<0.001$
O14907	Tax1-binding protein 3 OS=Homo sapiens GN=TAX1BP3 PE=1 SV=2 - [TX1B3_HUMAN]	124	13.7261295	0.62476735	$p<0.001$
O14745	Na(+)/H(+) exchange regulatory cofactor NHE-RF1 OS=Homo sapiens GN=SLC9A3R1 PE=1 SV=4 - [NHRF1_HUMAN]	358	38.844612	0.6105772	$p<0.001$
A0A096LPF0	Ras-related protein Rab-7b (Fragment) OS=Homo sapiens GN=RAB7B PE=4 SV=1 - [A0A096LPF0_HUMAN]	91	10.3803502	0.59567283	$p<0.001$
Q8IVL1	Neuron navigator 2 OS=Homo sapiens GN=NAV2 PE=1 SV=3 - [NAV2_HUMAN]	2,488	268.002547	0.58546377	$p<0.001$
Q9UKY7	Protein CDV3 homolog OS=Homo sapiens GN=CDV3 PE=1 SV=1 - [CDV3_HUMAN]	258	27.3183615	0.56625057	$p<0.001$
B4DEY6	LIM and cysteine-rich domains protein 1 OS=Homo sapiens GN=LMCD1 PE=2 SV=1 - [B4DEY6_HUMAN]	253	28.4947789	0.56611995	$p<0.01$
P49006	MARCKS-related protein OS=Homo sapiens GN=MARCKSL1 PE=1 SV=2 - [MRP_HUMAN]	195	19.5172325	0.56466249	$p<0.01$
P36405	ADP-ribosylation factor-like protein 3 OS=Homo sapiens GN=ARL3 PE=1 SV=2 - [ARL3_HUMAN]	182	20.44276	0.56320138	$p<0.001$
Q9Y2T7	Y-box-binding protein 2 OS=Homo sapiens GN=YBX2 PE=1 SV=2 - [YBOX2_HUMAN]	364	38.4947655	0.55489064	$p<0.01$
H0YE40	CD44 antigen (Fragment) OS=Homo sapiens GN=CD44 PE=1 SV=1 - [H0YE40_HUMAN]	82	9.09947282	0.51939027	$p<0.001$
P06401	Progesterone receptor OS=Homo sapiens GN=PGR PE=1 SV=4 - [PRGR_HUMAN]	933	98.9181716	0.5090052	$p<0.001$
Q02790	**Peptidyl-prolyl cis-trans isomerase FKBP4 OS=Homo sapiens GN=FKBP4 PE=1 SV=3 - [FKBP4_HUMAN]**	**459**	**51.7720738**	**0.48439102**	$p<0.001$
P08185	Corticosteroid-binding globulin OS=Homo sapiens GN=SERPINA6 PE=1 SV=1 - [CBG_HUMAN]	405	45.1119093	0.39363177	$p<0.001$
Q9H993	UPF0364 protein C6orf211 OS=Homo sapiens GN=C6orf211 PE=1 SV=1 - [CF211_HUMAN]	441	51.1398629	0.37407832	$p<0.001$
P02795	Metallothionein-2 OS=Homo sapiens GN=MT2A PE=1 SV=1 - [MT2_HUMAN]	61	6.0371964	0.33853248	$p<0.001$

were significantly increased while proteins involved in the PI3K/Akt/mTOR pathway (Akt and mTOR) were unchanged. It was interesting that signaling components of the Ras pathway (*i.e.*, MEK and ERK1) were unchanged, while the downstream effectors (*i.e.*, RSK1 and RSK2) of the Ras and p38/MAPK pathway were the predominant kinases that were increased. In general, RSK phosphorylates various substrates that control diverse cellular processes and when inhibited, it

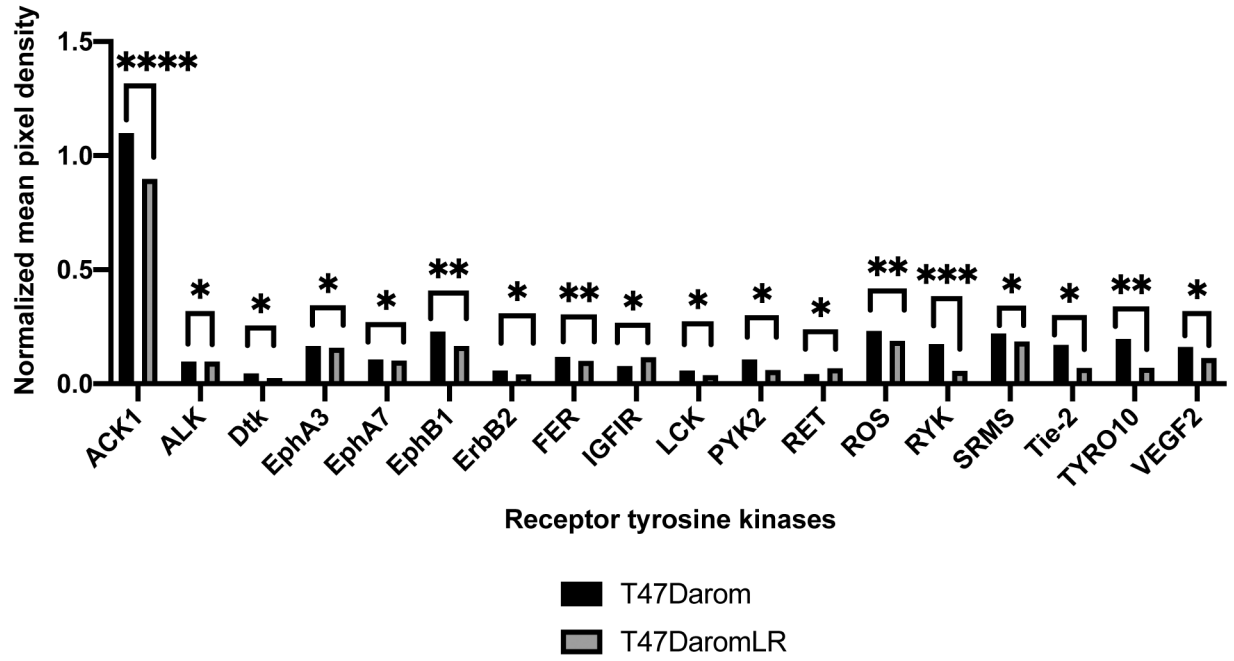

Figure 2. *Hormone dependent letrozole resistance induces global down-regulation of activated receptor tyrosine kinases. Graph depict normalized mean pixel density of protein levels in lysates prepared from the T47Darom and T47DaromLR cells using the Human RTK Antibody Array Membrane where 71 different anti-RTK antibodies were spotted in duplicated, including 4 positive and 3 negative controls and 1 blank. Array signals were analyzed using Image Lab (BioRad) software. Values from duplicate spots were averaged and plotted. Results are expressed as the mean unit±SD (****p<0.0001, ***p<0.001, **p<0.01, *p<0.05).*

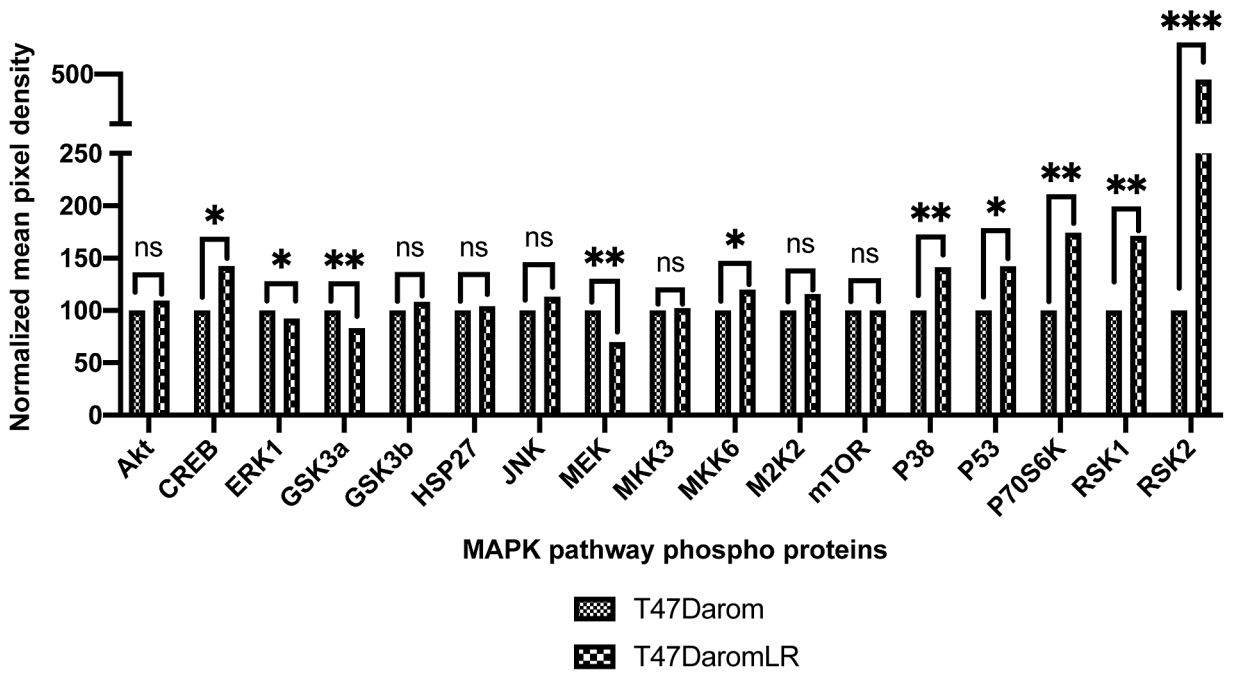

Figure 3. *MAPK signaling cascade is induced in the letrozole-resistant T47DaromLR cells. Graph depict normalized mean pixel density of protein levels in lysates prepared from the T47Darom and T47DaromLR cells using the Human MAPK Phosphorylation Antibody Array Membrane where 17 different anti-MAPK related antibodies were spotted in duplicate, including 4 positive and 3 negative controls and 1 blank. Array signals were analyzed using Image Lab (BioRad) software. Values from duplicate spots were averaged and plotted. Results are expressed as the mean unit±SD (***p<0.001, **p<0.01, *p<0.05).*

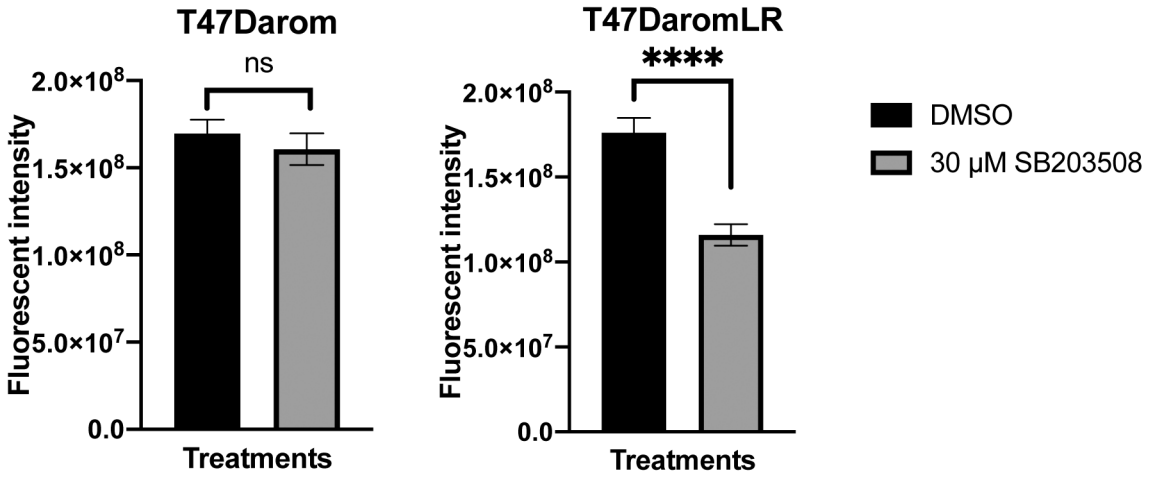

Figure 4. *Letrozole resistant cells are more sensitive to the growth inhibitory effects of p38/MAPK inhibitor SB 203508. The T47Darom cells were cultured in standard growth media and transferred to phenol red free media for two days prior to treatment with DMSO control or 30 μM of SB 203508 and cell proliferation assays were performed after 24 h. Proliferation was measured using the resazurin assay and graphs depict the fluorescence intensity of cells read at 430/560 nM wavelengths. Results are expressed as the mean unit±SD (****p<0.0001) of three independent experiments in triplicate; ns: not significant.*

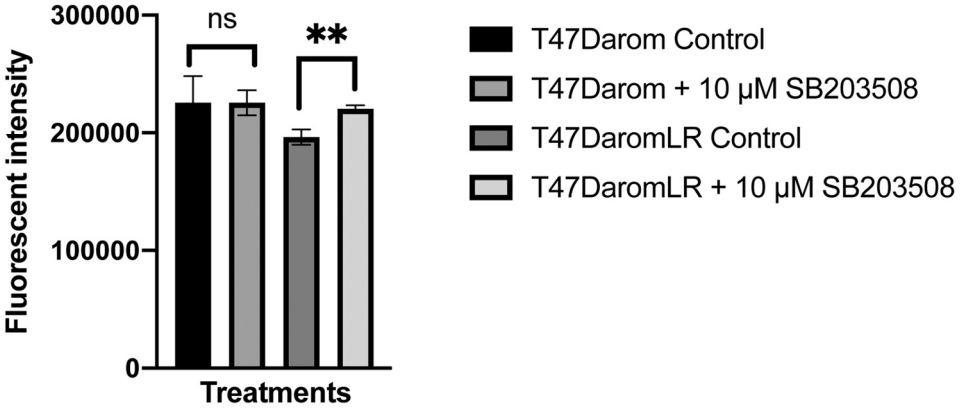

Figure 5. *Induction of apoptosis through targeting p38. The T47Darom cells were cultured in standard growth media and transferred to phenol red free media for two days prior to treatment with DMSO control or 10 μM of SB 203508 and caspase 3/7 activity was assessed by measuring the fluorescent intensity of cells at 530/502 nM wavelength. Results are expressed as the mean unit±SD (**p<0.01) of three independent experiments in triplicate.*

eliminates breast tumor initiating cells which are *de novo* chemo-resistant (16). Given these findings, it is likely that ER-dependent AI resistance is mediated through the p38/MAPK signaling cascade. The observation that the MAPK signaling was increased in the T47DaromLR cells was not completely novel, since it has been previously reported that HER2, p-Shc, Grb2, and the signaling proteins in the MAPK cascade were increased in the LTLT-Ca cells (1).

A global proteomic analysis was conducted using the T47Darom and the T47DaromLR cells to further identify a protein signature specifically associated with ER+ AI resistance. Since we identified that acquired resistance was associated with the p38/MAPK signaling cascade, it is notable that one of the upstream signaling molecules, MAP3K6 was up-regulated. Out of a total of 127 significantly increased proteins, MAP3K6 exhibited the highest expression and was associated with decreased relapse-free survival. This further underscored the aggressive nature of breast tumors fitting this profile. Based on these findings, it is likely that as letrozole sensitive cells transition to a letrozole resistant phenotype they preferentially proliferate through activation of the p38/MAPK pathway

inducing phosphorylation of RSK1/RSK2. Failure of these cells to respond to tamoxifen suggests they may utilize additional ligand independent signaling mechanism potentiated by p38. When the cells were treated with a p38 inhibitor, the T47Darom cells exhibited decreased proliferation and a slight induction in apoptosis.

While the major focus of this study was the p38/MAPK pathway, other proteins were identified including a protein disulfide isomerase (PDI) P4HB (prolyl 4-hydroxylase b). During times of oxidative stress or endoplasmic reticulum stress proteins unfold and molecular chaperones, like P4HB, assist in restoring unfolded proteins to their native conformation (17). A previous report has found that P4HB promoted a malignant phenotype in glioma cells *via* MAPK signaling (18) and identified P4HB as a novel target of chemoresistance in glioblastoma multiforme (19). It was hypothesized that perturbation of P4HB may sensitize the chemo-resistant glioma cells. While it is also known that PDIs serve as molecular chaperones to maintain ERα structure and function (20), the significance of high levels of P4HB and/or convergence with MAPK signaling pathways in AI-resistance remains unclear.

The proteomic analysis also revealed increased midasin (MDN1) expression which functions as a nuclear chaperone that is involved in the assembly/disassembly of macromolecular complexes in the nucleus, and is associated with maturation of 60S ribosome subunits (21). The finding that midasin was overexpressed in the T47DaromLR cells was interesting because a previous proteomic analysis demonstrated a 35-fold increase in MDN1 expression in LTLT-Ca cells cultured as mammospheres compared to LTLT-Ca cells cultured adherently (22, 23). While the role of midasin in breast cancer remains unclear, it is known that ribosomal biogenesis remains at the heart of translation. This process requires extensive regulation and coordination to meet the cellular demands of continuous ribosome production and aberrant midasin expression and subsequent interference with ribosomal biogenesis affects translation and the overall fitness of the cell.

While the proteomic signature of ER+ AI resistance is associated with enhanced p38/MAPK signaling there are additional factors contributing to this phenotype that are yet to be understood. Future studies will allow understanding how various signaling cascades converge to induce acquired letrozole resistance.

Conflicts of Interest

The Authors declare no conflicts of interest in relation to this study.

Authors' Contributions

SLT conceived and designed the experiments and directed the project. RRW and MRB performed the experiments. AMD, KPL, and GW contributed to data acquisition. RRW, KZ, and KMG analyzed and interpreted the data. AMD provided technical editing. RRW and SLT wrote the manuscript.

Acknowledgements

The Authors thank the ITT Research Institute and Dr. Akash Gupta for generously donating the T47Darom and T47DaromLR cell lines.

Funding

This work was supported in part by the National Institutes of Health [grant number 1SC1GM126617] awarded to Syreeta L. Tilghman. This publication was made possible by funding from the Louisiana Cancer Research Consortium and the National Institutes of Health Research Centers at Minority Institutes [grant numbers 8G12MD007595 and U54MD007582] from the National Institute on Minority Health and Health Disparities. The contents are solely the responsibility of the authors and do not necessarily represent the official views of the Louisiana Cancer Research Consortium or the NIH.

References

1 Jelovac D, Sabnis G, Long BJ, Macedo L, Goloubeva OG and Brodie AM: Activation of mitogen-activated protein kinase in xenografts and cells during prolonged treatment with aromatase inhibitor letrozole. Cancer Res *65(12)*: 5380-5389, 2005. PMID: 15958587. DOI: 10.1158/0008-5472.can-04-4502

2 Tilghman SL, Townley I, Zhong Q, Carriere PP, Zou J, Llopis SD, Preyan LC, Williams CC, Skripnikova E, Bratton MR, Zhang Q and Wang G: Proteomic signatures of acquired letrozole resistance in breast cancer: Suppressed estrogen signaling and increased cell motility and invasiveness. Mol Cell Proteomics *12(9)*: 2440-2455, 2013. PMID: 3769322. DOI: 10.1074/mcp.M112.023861

3 Gupta A, Mehta R, Alimirah F, Peng X, Murillo G, Wiehle R and Mehta RG: Efficacy and mechanism of action of proellex, an antiprogestin in aromatase overexpressing and letrozole resistant T47D breast cancer cells. J Steroid Biochem Mol Biol *133*: 30-42, 2013. PMID: 22939887. DOI: 10.1016/j.jsbmb.2012.08.004

4 Győrffy B, Lanczky A, Eklund AC, Denkert C, Budczies J, Li Q and Szallasi Z: An online survival analysis tool to rapidly assess the effect of 22,277 genes on breast cancer prognosis using microarray data of 1,809 patients. Breast Cancer Res Treat *123(3)*: 725-731, 2010. PMID: 20020197. DOI: 10.1007/s10549-009-0674-9

5 Johnson KP, Yearby LA, Stoute D, Burow ME, Rhodes LV, Gray M, Carriere P, Tilghman SL, McLachlan JA and Ochieng J: *In vitro* and *in vivo* evaluation of novel anticancer agents in triple negative breast cancer models. J Health Care Poor Underserved 24: 104-111, 2013. PMID: 3628744. DOI: 10.1353/hpu.2013.0047

6 Walker RR, Patel J, Davidson AM, and Tilghman SL: A novel phytoalexin, glyceollins, trigger anti-proliferative effects in aromatase inhibitor resistant breast cancer. Cancer Res *80(16 Suppl)*: Abstract 4116, 2020. DOI: 10.1158/1538-7445.AM2020-4116

7 Sabnis G and Brodie A: Adaptive changes results in activation of alternate signaling pathways and resistance to aromatase inhibitor resistance. Mol Cell Endocrinol *340(2)*: 142-147, 2011. PMID: 20849912. DOI: 10.1016/j.mce.2010.09.005

8 Lotem J and Sachs L: A mutant p53 antagonizes the deregulated c-myc-mediated enhancement of apoptosis and decrease in leukemogenicity. Proc Natl Acad Sci USA *92(21)*: 9672-9676, 1995. PMID: 7568195. DOI: 10.1073/pnas.92.21.9672

9 Li R, Sutphin PD, Schwartz D, Matas D, Almog N, Wolkowicz R, Goldfinger N, Pei H, Prokocimer M and Rotter V: Mutant p53 protein expression interferes with p53-independent apoptotic pathways. Oncogene *16(25)*: 3269-3277, 1998. PMID: 9681826. DOI: 10.1038/sj.onc.1201867

10 Blandino G, Levine AJ and Oren M: Mutant p53 gain of function: Differential effects of different p53 mutants on resistance of cultured cells to chemotherapy. Oncogene *18(2)*: 477-485, 1999. PMID: 9927204. DOI: 10.1038/sj.onc.1202314

11 Bergamaschi D, Gasco M, Hiller L, Sullivan A, Syed N, Trigiante G, Yulug I, Merlano M, Numico G, Comino A, Attard M, Reelfs O, Gusterson B, Bell AK, Heath V, Tavassoli M, Farrell PJ, Smith P, Lu X and Crook T: P53 polymorphism influences response in cancer chemotherapy *via* modulation of p73-dependent apoptosis. Cancer Cell *3(4)*: 387-402, 2003. PMID: 12726864. DOI: 10.1016/s1535-6108(03)00079-5

12 Matas D, Sigal A, Stambolsky P, Milyavsky M, Weisz L, Schwartz D, Goldfinger N and Rotter V: Integrity of the n-terminal transcription domain of p53 is required for mutant p53 interference with drug-induced apoptosis. EMBO J *20(15)*: 4163-4172, 2001. PMID: 11483519. DOI: 10.1093/emboj/20.15.4163

13 Murphy KL, Dennis AP and Rosen JM: A gain of function p53 mutant promotes both genomic instability and cell survival in a novel p53-null mammary epithelial cell model. FASEB J *14(14)*: 2291-2302, 2000. PMID: 11053251. DOI: 10.1096/fj.00-0128com

14 Aas T, Børresen AL, Geisler S, Smith-Sørensen B, Johnsen H, Varhaug JE, Akslen LA and Lønning PE: Specific p53 mutations are associated with *de novo* resistance to doxorubicin in breast cancer patients. Nat Med *2(7)*: 811-814, 1996. PMID: 8673929. DOI: 10.1038/nm0796-811

15 Sabnis G, Schayowitz A, Goloubeva O, Macedo L and Brodie A: Trastuzumab reverses letrozole resistance and amplifies the sensitivity of breast cancer cells to estrogen. Cancer Res *69(4)*: 1416-1428, 2009. PMID: 2644349. DOI: 10.1158/0008-5472.can-08-0857

16 Stratford AL, Reipas K, Hu K, Fotovati A, Brough R, Frankum J, Takhar M, Watson P, Ashworth A, Lord CJ, Lasham A, Print CG and Dunn SE: Targeting p90 ribosomal s6 kinase eliminates tumor-initiating cells by inactivating y-box binding protein-1 in triple-negative breast cancers. Stem Cells *30(7)*: 1338-1348, 2012. PMID: 22674792. DOI: 10.1002/stem.1128

17 Noiva R: Protein disulfide isomerase: The multifunctional redox chaperone of the endoplasmic reticulum. Semin Cell Dev Biol *10(5)*: 481-493, 1999. PMID: 10597631. DOI: 10.1006/scdb.1999.0319

18 Sun S, Kiang KMY, Ho ASW, Lee D, Poon MW, Xu FF, Pu JKS, Kan ANC, Lee NPY, Liu XB, Man K, Day PJR, Lui WM, Fung CF and Leung GKK: Endoplasmic reticulum chaperone prolyl 4-hydroxylase, beta polypeptide (p4hb) promotes malignant phenotypes in glioma *via* mapk signaling. Oncotarget *8(42)*: 71911-71923, 2017. PMID: 29069756. DOI: 10.18632/oncotarget.18026

19 Sun S, Lee D, Ho AS, Pu JK, Zhang XQ, Lee NP, Day PJ, Lui WM, Fung CF and Leung GK: Inhibition of prolyl 4-hydroxylase, beta polypeptide (P4HB) attenuates temozolomide resistance in malignant glioma *via* the endoplasmic reticulum stress response (ERSR) pathways. Neuro Oncol *15(5)*: 562-577, 2013. PMID: 23444257. DOI: 10.1093/neuonc/not005

20 Schultz-Norton JR, McDonald WH, Yates JR and Nardulli AM: Protein disulfide isomerase serves as a molecular chaperone to maintain estrogen receptor alpha structure and function. Mol Endocrinol *20(9)*: 1982-1995, 2006. PMID: 16690750. DOI: 10.1210/me.2006-0006

21 Garbarino JE and Gibbons IR: Expression and genomic analysis of midasin, a novel and highly conserved aaa protein distantly related to dynein. BMC Genomics *3*: 18, 2002. PMID: 12102729.

22 Tilghman SL, Pratt J, Llopis SD, Davidson AM, Walker RR, Carriere P, Davenport IR, Zhang W and Zhang K: Abstract 3183: Proteomic characterization of aromatase inhibitor resistant mammospheres reveal the presence of a novel nuclear chaperone. Cancer Res 77, 2017. DOI: 10.1158/1538-7445.AM2017-3183

23 Gallegos KM, Patel JR, Llopis SD, Walker RR, Davidson AM, Zhang W, Zhang K, and Tilghman SL: Quantitative proteomic profiling identifies a potential novel chaperone marker in resistant breast cancer. Front Oncol 2021 [epub ahead of print]. DOI: 10.3389/fonc.2021.540134

Received November 30, 2020
Revised December 31, 2020
Accepted January 4, 2021